77th IIW Annual Assembly and International Conference on Welding and Joining 7-12 July 2024 Rhodes, Greece

Hardness Prediction of the Heat-Affected Zone in Multilayer Welded Austenitic Stainless Steel Based on Dislocation Density Change Behavior

Lina Yu[1,*], *Kazutoshi* Nishimoto[1], *Hiroyuki* Hirata[1], and *Kazuyoshi* Saida[1]

[1] Graduate School of Engineering, Osaka University, Japan

Abstract. The effects of strain hardening and recovery/recrystallization on the hardness of the heat-affected zone (HAZ) in multilayer welded austenitic stainless steel SUS316 were investigated in this study. The results revealed that strain hardening due to welding strain and softening due to recovery/recrystallization were the dominant factors affecting the hardness change in the HAZ during multilayer welding process. Furthermore, the relationship between the strain and dislocation density and that between the recovery/recrystallization and dislocation density were quantitatively investigated using positron annihilation lifetime spectroscopy. Based on these results, a new hardness prediction method based on the change in dislocation density in the HAZ during multilayer welding was proposed. The hardness values in the HAZ after the multilayer welding were predicted based on the simulated strain and thermal history, and the calculated hardness values agreed well with the measured results. This indicates that the newly proposed hardness prediction method based on the dislocation density change behavior in the HAZ during multilayer welding is valuable and effective for selecting the appropriate welding conditions before actual welding.

1. Introduction

Stress corrosion cracking (SCC) in welded components of austenitic stainless steel is one of the significant aging degradation problems in nuclear power plants. SCC is caused by the superimposition of material, stress, and environmental factors [1,2]. For the material factor, low-carbon stainless steel was developed and applied as a countermeasure to prevent sensitization caused by chromium carbide precipitation [3,4]. However, in recent years, SCC has been confirmed to occur near the welds of low-carbon austenitic stainless steel pipes, even in areas where sensitization has not occurred [5,6]. Subsequent studies reported that when hardening occurred in the material, the SCC susceptibility [7,8] and SCC growth rate increased [9], regardless of the presence or absence of sensitization. Because hardening has also been confirmed in welded components where SCC occurred, the hardening phenomenon due to welding has attracted attention.

Austenitic stainless steel has a strong tendency for strain hardening owing to its fcc crystal structure and low stacking fault energy. High plastic strain can accumulate during a multilayer welding process. On the other hand, the accumulated strain hardening can be reduced or even eliminated during the welding thermal cycle owing to recovery/recrystallization and grain growth. For austenitic stainless steels, the effects of strain hardening [10], recovery/recrystallization [11], dynamic strain aging [12,13], and other phenomena related to the hardness change have been studied. However, hardening in the welded HAZ has been studied primarily from a mechanical viewpoint, focusing only on stress and strain; few studies from a material viewpoint are available. Therefore, the hardening mechanism in a multilayer-welded HAZ has not yet been clarified. To elucidate the hardening mechanism, the dominant factor affecting the hardness change in the HAZ is to be clarified first. Furthermore, hardness prediction in the multilayer welded HAZ based on the hardening mechanism before the actual welding is crucial for welding safety.

Therefore, herein, the effect of each phenomenon on the change in hardness was investigated by tensile and thermal aging tests on pre-strained materials simulating the HAZ in austenitic stainless steel JIS SUS316. The hardening mechanism in the multilayer-welded HAZ was also discussed from the material viewpoint. The essence of hardness is the ease of dislocation movements mainly due to changes in dislocation density. When multiple phenomena are considered at the same time, it's necessary to discuss the relationship between the phenomena with dislocation density. Therefore, the relationship between the dominant phenomena of hardness change and dislocation density was quantitatively investigated using the positron annihilation lifetime method. Based on the observed results, a new hardness prediction method based on the dislocation density change behavior in the HAZ during multilayer welding was proposed, and the validity of the prediction method was experimentally verified.

2. Materials and Methods

In this study, austenitic stainless steel SUS316 was used as the base material, and YS316 was used as the welding wire; their chemical compositions are listed in Table 1.

Table 1 Chemical compositions of materials (mass%)

Material	C	Si	Mn	P	S	Ni	Cr	Mo	Co	Fe
SUS316	0.04	0.60	0.93	0.034	0.004	10.16	16.83	2.06	0.20	Bal.
YS316	≦0.08	≦0.65	1.0-2.5	≦0.03	≦0.03	11.0-14.0	18.0-20.0	2.0-3.0	-	Bal.

Tensile tests were performed at room temperature to investigate the strain hardening behavior of SUS316. The shape of the tensile test piece is illustrated in Fig. 1. The strain rate was set as 4.2×10^{-5} s^{-1} to investigate the relationship between strain and dislocation density, and the relationship between dislocation density and hardness.

A pre-strained material simulating the strain caused by welding was fabricated to study the recovery and recrystallization phenomena. To improve uniformity and prevent temperature rise during rolling, the plate material was cold-rolled by 20% using multi-pass rolling at low speed and low reduction rate. The test pieces were cut from the central part of the rolled sample using electrical discharge machining, which would cause the minimal damage to the original state of the material.

The specimens were subjected to various heat treatments to investigate the hardness and dislocation density reduction behaviors due to recovery and recrystallization. The simulated HAZ thermal cycles were applied to a 20%-rolled sample using a high-frequency induction heating apparatus. The heating rate was 100 °C/s, and the peak temperature was varied from 600 to 1300 °C with a holding time of 1 s and then cooled at a cooling rate of approximately 50 °C/s in an atmosphere of pure argon. For the kinetic study of the dislocation density reduction behavior owing to recovery and recrystallization, the samples were thermally aged at 300–950 °C for various holding times with water cooling for all cases.

Vickers hardness tests were conducted to study the changes in hardness owing to each phenomenon. After polishing, the Vickers hardness at the center of the tensile specimen was measured under a load of 0.098 N for 15s, and the average value, excluding the maximum and minimum values, was obtained from multiple measurements.

Positron annihilation lifetime spectroscopy (PALS) is a non-destructive method that enables the nano-scale characterization of open-volume defects such as atomic vacancies and dislocations [14, 15]. PALS was used to characterize the lattice defects in the samples. A Na-22 thin-film NA351 positron source was used as the positron beam source, and the positron lifetime was measured in an atmosphere at room temperature sandwiched between two samples.

A TIG multilayer welding test was performed on SUS316 using the wire of YS316, with the welding conditions listed in Table 2. The thermal history and strain in the multilayer welds were simulated using FEM simulation software JWRIAN, which was specifically developed for predicting the thermal history, residual stress, and deformation of welds [16, 17].

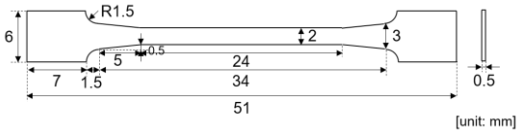

Fig. 1 Tensile specimen for tensile test.

Table 2 Welding conditions for multilayer welding.

Layer	Pass	Current (A)	Voltage (V)	Wire feed rate (mm/s)	Welding speed (mm/s)
1	1	250	15–16	45	1.67
2	2	220	14–15	45	1.67
3	3~4	220	14–15	45	1.67
4	5~6	220	14–15	45	1.67
5	7~8	220	14–15	45	1.67
6	9~10	220	14–15	45	1.67
7	11~13	220	14–15	45	1.67

3. Factors affecting the hardness change in multilayer welded HAZ

The effect of weld-induced strain on the hardness change in the HAZ was investigated. After the tensile tests at room temperature with various strains, hardness measurements were performed on each specimen to investigate the relationship between plastic strain and hardness. Fig. 2 shows the relationship between the equivalent plastic strain and Vickers hardness. The Vickers hardness was the average value obtained from multiple measurements, and the error bars showed the difference between the maximum/minimum value and the average value.

The hardness significantly increased with increasing equivalent plastic strain. Although the welding strain in the multilayer welded HAZ differs depending on the welding conditions, welding shapes, and other factors, a maximum welding strain of ~20%–25% can be introduced into the multilayer welded HAZ [18, 19]. This suggests that the strain introduced in the multilayer welded HAZ can cause an increase in the hardness by ~100 HV, indicating that strain hardening by weld strain significantly affects the hardness change in the multilayer welded HAZ.

To investigate the effect of recovery and recrystallization caused by the thermal cycle during welding on hardness change, the pre-strained 20%-rolled specimens simulating welding strain were heated at various peak temperatures with a holding time of 1 s to simulate the thermal cycles in HAZ. Vickers hardness measurements were performed after the thermal treatment, and the hardness results are shown in Fig. 3. In the figure, the hardness values before thermal treatment (309HV) and after solution treatment

(200HV) are indicated by dashed lines. The hardness decreased as the peak temperature increased and softened to the same level as the hardness of the base metal when the peak temperature was >1050 °C, even after thermal treatment for 1 s. This result suggests that the work-hardened areas due to welding would be softened owing to recovery and recrystallization during the welding thermal cycle.

The results in Figs. 2 and 3 suggest that strain hardening due to the welding strain and softening due to recovery/recrystallization are the dominant phenomena affecting the hardness change in the HAZ during the multilayer welding process.

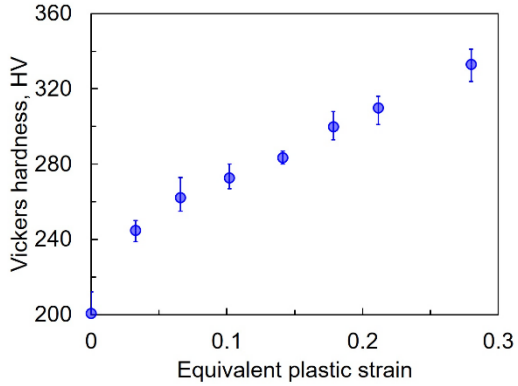

Fig. 2 Relationship between plastic strain and Vickers hardness at room temperature.

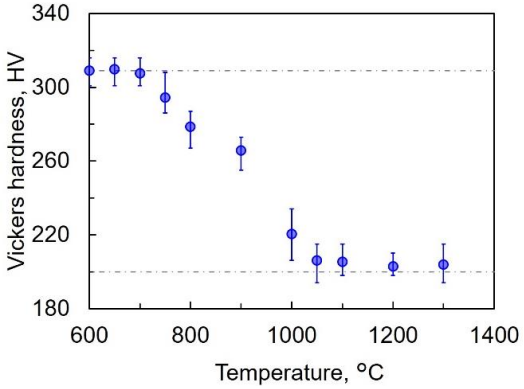

Fig. 3 Change of Vickers hardness due to heat treatment.

4. Dislocation density increase behavior due to strain

Fig. 4 shows the relationship between the equivalent plastic strain applied by the room-temperature tensile test and dislocation density. As the equivalent plastic strain increased, the dislocation density increased monotonically. The relationship between the equivalent plastic strain and dislocation density can be approximated by a straight line, and the relational expression is given by Eq. (1). Here, ρ is the dislocation density (m^{-2}), and ε_{eq} is the equivalent plastic strain.

$$\rho = (6.53 \times \varepsilon_{eq} + 0.0024) \times 10^{15} \qquad (1)$$

Fig. 5 shows the relationship between the hardness and dislocation density obtained in this study with the square root of the dislocation density. The relationship between the square root of the dislocation density and the hardness can be approximated by a straight line. As a result of deriving an approximation formula for the relationship between the dislocation density and hardness, the approximation formula is shown in Eq. (2). Here, HV is the Vickers hardness, and ρ is the dislocation density (m^{-2}).

$$HV = 3.13 \times 10^{-6} \times \left(\sqrt{\rho} - 1.23 \times 10^{6}\right) + 200 \qquad (2)$$

Using the expressions obtained above, the increase in dislocation density during plastic deformation in SUS316 was quantitatively calculated, and the strain hardening behavior owing to the increase in dislocation density could also be predicted.

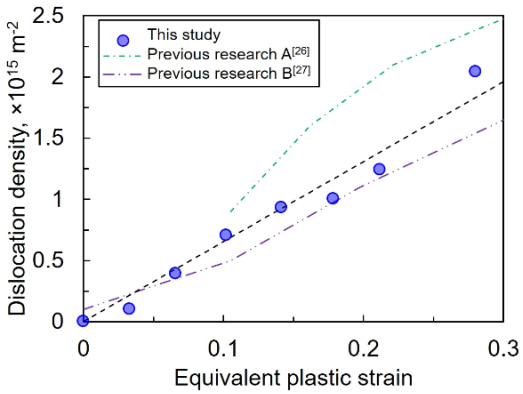

Fig. 4 Relationship between equivalent plastic strain and dislocation density.

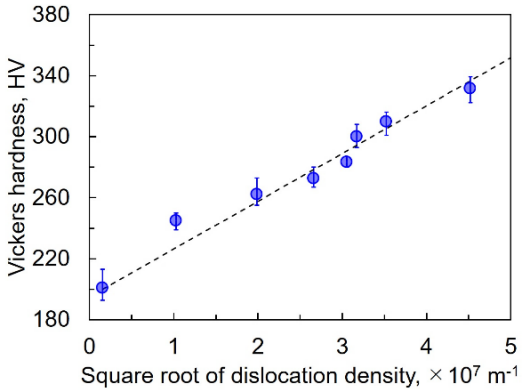

Fig. 5 Relationship between the square root of dislocation density and Vickers hardness.

5. Dislocation density reduction behavior due to recovery/recrystallization

Fig. 6 shows the dislocation density measured after thermal aging. In the conditions with peak temperature <600 °C, the dislocation density decreased monotonically with increasing thermal aging holding time, and after long-term aging, the dislocation density showed a constant value higher than that of the base metal. At thermal aging temperatures >850 °C, the dislocation density decreased monotonically with

increasing holding time and decreased to the same level as the base metal after long-term thermal aging.

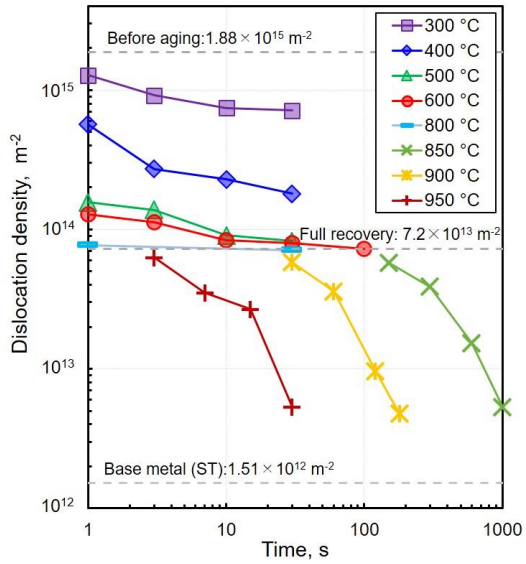

Fig. 6 Dislocation reduction behavior due to thermal aging.

To understand the dislocation density reduction behavior due to the recovery/recrystallization phenomenon, the dislocation density reduction behavior during thermal aging at 300–600 °C was kinetically analyzed. In a previous study [20], the hardness reduction behavior owing to recovery was kinetically analyzed, and when the recovery fraction was defined by Eq. (3), it was found that the hardness reduction behavior owing to recovery follows the Johnson–Mehl equation [21-23] (Eq. (4)). Here, HV_{before}: the hardness before aging, HV_{after}: the hardness after the completion of recovery, HV_{aged}: the hardness after thermal aging, f: the recovery fraction, K: the rate constant (s^{-1}), t: the time (s), and n: the exponent.

$$f = \frac{HV_{before} - HV_{aged}}{HV_{before} - HV_{after}} \quad (3)$$

$$f = 1 - \exp\{-(Kt)^n\} \quad (4)$$

Because a close correlation exists between the dislocation density and hardness, the ecovery/recrystallization behavior can be similarly analyzed by defining the dislocation density reduction rate owing to recovery, as in Eq. (5). Here, ρ_{before}: dislocation density before aging (m^{-2}), ρ_{after}: dislocation density after completion of recovery (m^{-2}), and ρ_{aged}: dislocation density after thermal aging (m^{-2}).

$$f = \frac{\rho_{before} - \rho_{aged}}{\rho_{before} - \rho_{after}} \quad (5)$$

In addition, by taking the logarithms of both sides of Eq. (4) and transforming it, it can be expressed as Eq. (6) below.

$$\ln\left\{\ln\left(\frac{1}{1-f}\right)\right\} = n\ln(t) + n\ln(K) \quad (6)$$

In general, the rate constant K obtained from the Johnson–Mehl plot can be expressed using Eq. (8) by taking the logarithms of both sides of Eq. (7). K_0: the rate constant (s^{-1}), Q: the activation energy, R: the gas constant (8.314 J/mol·K), and T: the temperature (K).

$$K = K_0 \exp\left(-\frac{Q}{RT}\right) \quad (7)$$

$$\ln(K) = \ln(K_0) - \frac{Q}{RT} \quad (8)$$

The measurement results for the 20%-rolled material suggested that the dislocation density decreased owing to the recovery phenomenon at low temperatures and recrystallization at high temperatures. Table 3 summarizes the constant values of n, Q, and K_0 obtained from the recovery and recrystallization kinetic analyses. The activation energy for recovery is much lower than that for recrystallization. The activation energy varied depending on the rate-determining mechanism of the phenomenon. This suggests that the rate-determining mechanisms for the dislocation density reduction behavior owing to recovery and recrystallization are different.

Table 3 Comparison of kinetic constants of dislocation reduction behavior due to recovery or recrystallization.

Constants	Recovery	Recrystallization
n	0.2010	1.3539
Q (kJ/mol)	122.9	393.5
K_0 (s^{-1})	1.53×10^{10}	4.68×10^{15}

6. Hardness prediction method based on dislocation density change behavior in multilayer welded HAZ

The results in Section 3 suggest that the dominant factors for HAZ hardening during multilayer welding are strain hardening and softening owing to recovery/recrystallization. In addition, the relationship between strain and dislocation density increase behavior, and the relationship between recovery/recrystallization and dislocation density reduction behavior are quantitatively investigated in Sections 4 and 5, respectively. Subsequently, the dislocation density change behavior due to each phenomenon is clarified. However, in the HAZ, the increase in dislocation density owing to strain and reduction in dislocation density due to recovery/recrystallization co-occur at the same time. Therefore, to quantitatively predict the dislocation density change behavior in the HAZ, a new theoretical model was proposed in this study for simultaneously calculating the dislocation density increase behavior due to strain and dislocation density reduction behavior due to recovery/recrystallization.

Fig. 7 shows a flowchart of the dislocation density change calculation owing to strain and recovery/recrystallization, which is proposed in this study. Based on the simulated thermal history and weld strain history at each grid node, the dislocation density was calculated.

In this study, 7 layer - 13 pass welded sample was used to verify the effectiveness of the proposed hardness prediction system for multilayer welds. The

thermal cycles in the multilayer welds were simulated using the thermal elastic-plastic FEM software JWRIAN [16, 17]. Based on the actual cross section, the mesh model of 7-layer welds was created as shown in Fig. 8. A moving welding heat source was used in the welding analysis. The melting point of SUS316 steel is 1400 °C, and the temperature-dependent material properties [24] are shown in Fig. 9.

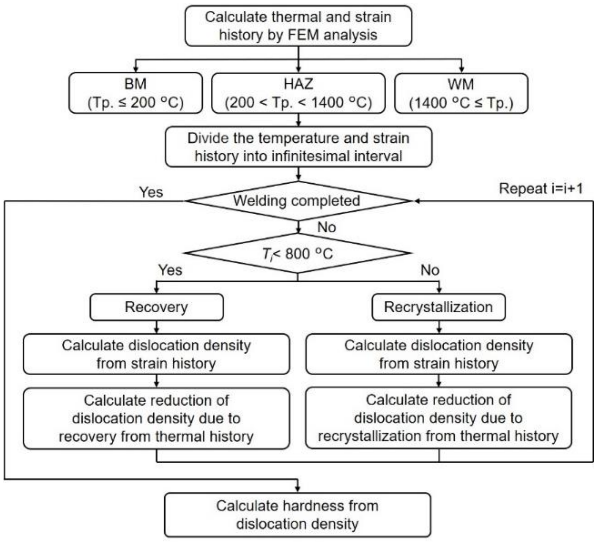

Fig. 7 Flowchart of hardness prediction in multilayer welded HAZ.

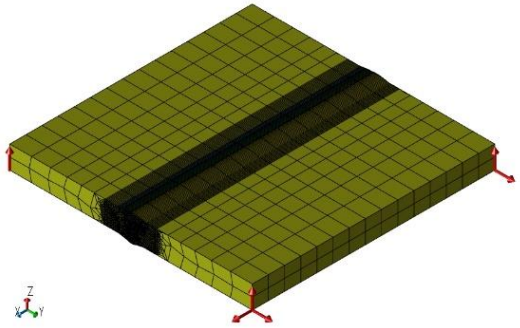

Fig. 8 FEM analysis model of multilayer welds.

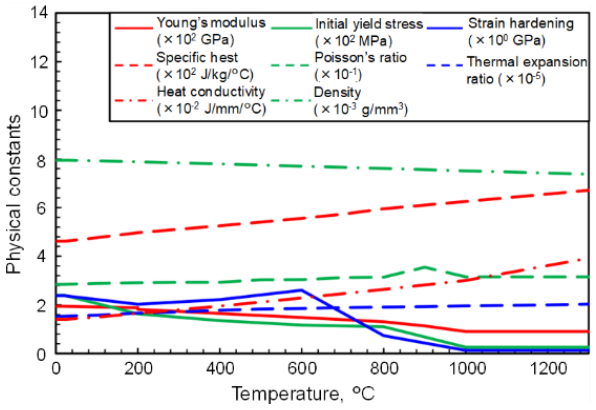

Fig. 9 Temperature-dependent material properties of SUS316.

Fig. 10 shows the simulated peak temperature distribution in the middle cross section after 7-layer welding. The simulated weld metal part is illustrated in red color with a peak temperature >1400 °C. The deformation of welds was also considered in the simulation, and the simulated shape of the weld metal matches that of the actual weld metal well, indicating that the FEM simulation results are appropriate. Fig. 11 shows the simulated equivalent plastic strain distribution in the cross section after 7-layer welding. The strain was high near the fusion boundary and under-surface.

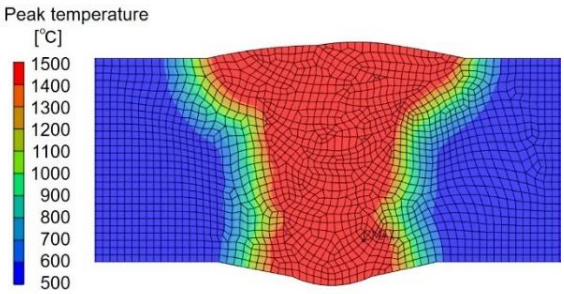

Fig. 10 Simulated peak temperature distribution after 7 layer - 13 pass welding.

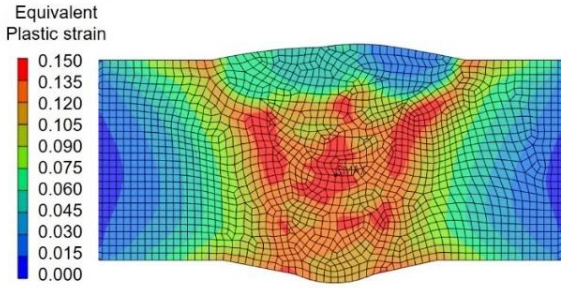

Fig. 11 Simulated equivalent plastic strain distribution after 7 layer - 13 pass welding.

Based on the simulated thermal history and equivalent plastic strain history of each grid node, the hardness values in the HAZ were calculated using the proposed method. Because the temperature distribution shown in Fig. 10 was generally symmetrical, the hardness distribution was observed only on the right side of the welding cross section. Fig. 12(a) presents the predicted hardness distribution in the HAZ as a color chart map, with the hardness values displayed in rainbow colors for different hardness levels calculated using the method proposed in this study.

To verify the validity of the proposed hardness prediction method for multilayer welds, the hardness was experimentally measured in an actual welded cross section as shown in in Fig. 12(b). It is found that hardening is observed near the fusion boundary and under-surface, and no change in the hardness of the base metal was observed further away. Near the final layer weld, there were areas near the fusion boundary where the hardness was almost the same as that of the base material, and hardening was observed slightly away from the fusion boundary. The predicted hardness distribution shown in Fig. 12(a) agreed well with the experimentally measured results, both in terms of the hardness value and overall tendency.

These results indicate that the proposed hardness prediction method based on the dislocation density change behavior, which considers both strain and recovery/recrystallization, is valuable and effective. Therefore, appropriate welding conditions can be selected before actual multilayer welding, which is useful for multilayer welding in industry.

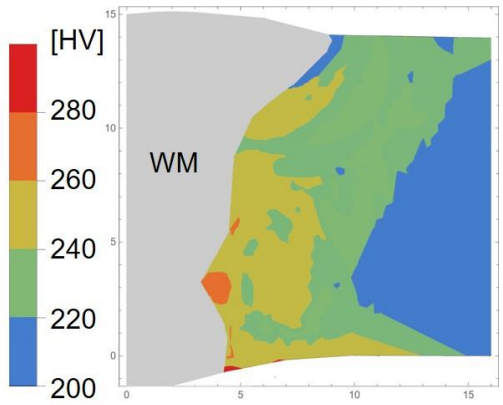

(a) Predicted hardness distribution by proposed method

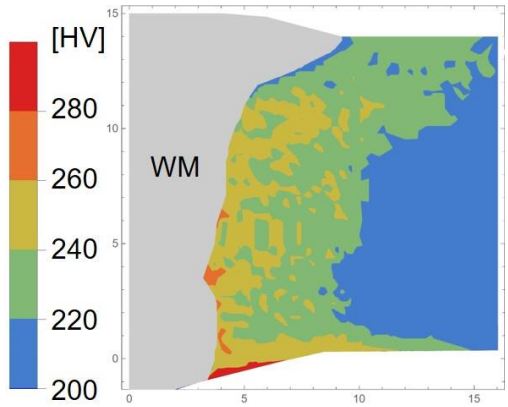

(b) Measured hardness distribution

Fig. 12 Comparison of measured and predicted hardness distributions after multilayer welding

7. Conclusions

(1) The hardness results suggested that strain hardening due to welding strain and softening due to recovery/recrystallization were the dominant phenomena affecting the hardness change in the HAZ during the multilayer welding process.

(2) The increase in dislocation density due to strain was analyzed by PALS. The relationship between the square root of the dislocation density and hardness was approximated by a straight line, and a relational expression between the dislocation density and hardness was obtained.

(3) The decrease in dislocation density due to recovery at low temperatures and recrystallization at high temperatures was kinetically studied using the Johnson–Mehl equation and Arrhenius equation.

(4) A new hardness prediction method was proposed based on the coupled prediction of the increase in dislocation density due to strain and the decrease in dislocation density due to recovery/recrystallization.

(5) The predicted hardness results correspond well with the measured results, indicating that the proposed hardness prediction method is valuable and effective for selecting appropriate welding conditions before actual welding.

References

[1] K. Sieradzki, R.C. Newman, J. Phys. Chem. Solids, **48**, pp. 1101–1113 (1987)

[2] X. Xie, D. Ning, B. Chen, S. Lu, J. Sun, Corros. Sci., **12**, 576–584 (2016)

[3] K. Takamori, S. Suzuki, K. Kumagai, Maintenology, **3**, 52–58 (2004)

[4] M. Koshiishi, M. Okada, H. Fujimori, A. Hirano, Hitachi Rev., **91**, 214–217 (2009)

[5] S. Suzuki, K. Takamori, K. Kumagai, S. Ooki, T. Fukuda, H. Yamashita, T. Futami, Pres. Eng., J. Japan High Pres. Inst., **42**, 188–198 (2004)

[6] The Kansai Electric Power Co., Inc., Regarding Significant Indications at Ohi Power Station Unit 3 Pressurizer Spray Line Piping Welds, (2020)

[7] N. Ishiyama, M. Mayuzumi, Y. Mizutani, J. Tani, J. Japan Inst. Mater., **69**, 1049–1052 (2005)

[8] O. Raquet, E. Herms, F. Vaillant, T. Couvant, Adv. Mat. Sci., **7**, 33–46 (2007)

[9] T. Masuoka, M. Mayuzumi, T. Arai, J. Tani, Zairyo-to-Kankyo, **56**, 93–98 (2007)

[10] M. Aoki, T. Terachi, T. Yamada, K. Arioka: INSS J., **19**, 118–130 (2012)

[11] R. Ihara, T. Hashimoto, M. Mochizuki, J. Soc. Mat. Sci., Japan, **61**, 961–966 (2012)

[12] L. Yu, K. Nishimoto, K. Saida, J. Mat. Sci. Eng. A, **13**, 13–25 (2023)

[13] K. Kako, J. Ohta, M. Mayuzumi, J. Jap. Inst. Metals, **70**, 694–699 (2006)

[14] Y. C. Jean, Microchem. J., **42**, 72–102 (1990)

[15] B. Li, V. Krsjak, J. Degmova, Z. Wang, T. Shen, H. Li, S. Sojak, V. Slugen, A. Kawasuso, J. of Nucl. Mater., **535**, 152–180 (2020)

[16] D. Deng, H. Murakawa, M. Shibahara, Comp. Mat. Sci., **48**, 187–194 (2010)

[17] J. Park, G. An, N. Ma S. Kim, J. Manuf. Process., **102**, 182–194 (2023)

[18] P. L. Andresen, Corrosion, **9**, 1024–1038 (2013)

[19] S. Suzuki, K. Takamori, K. Kumagai, A. Sakashita, N. Yamashita, C. Shitara, Y. Okamura, E-J. Adv. Maint., **1**, 1–29 (2019)

[20] L. Yu, K. Saida, H. Araki, K. Sugita, M. Mizuno, K. Nishimoto, N. Chigusa, Mat. Sci. Eng. A, **796**, 140221 (2020)

[21] W. A. Johnson, K. F. Mehl, Trans. Am. Inst. Min. (Metall) Eng., **135**, 416–442 (1939)

[22] M. Avrami, J. Chem. Phys., **7**, 1103–1112 (1939)

[23] M. Fanfoni, M. Tomellini, IL NUOVO CIMENTO, **20D**, 1171–1182 (1998)

[24] D. Deng, S. Kiyoshima, Nucl. Eng. Des., **240**, 688–696 (2010)